Materials Horizons

ROYAL SOCIETY OF CHEMISTRY

COMMUNICATION

View Article Online
View Journal | View Issue



Cite this: *Mater. Horiz.*, 2023, **10**, 2945

Received 6th March 2023,
Accepted 4th May 2023

DOI: 10.1039/d3mh00341h

rsc.li/materials-horizons



# Self-healing liquid metal hydrogel for human–computer interaction and infrared camouflage†

Xiaofei Li,[ab] Miao Jiang,[ab] Yiming Du,[ab] Xin Ding,[a] Chao Xiao,[a] Yanyan Wang,[a] Yanyu Yang,[*c] Yizhi Zhuo,[a] Kang Zheng,[a] Xianglan Liu,[a] Lin Chen,[a] Yi Gong,[a] Xingyou Tian[ab] and Xian Zhang[*ab]

**Due to their mechanical flexibility, conductive hydrogels have been widely investigated in the fields of flexible electronics and soft robots, but their non-negligible disadvantages, such as poor toughness and limited self-healing, severally restrict their practical application. Herein, gallium indium alloy (EGaIn) is utilized to initiate the polymerization and simultaneously serve as flexible fillers to construct a super-stretchable and self-healing liquid metal/polyvinyl alcohol/*p*(acrylamide-*co*-octadecyl methacrylate) (liquid metal/PVA/P(AAm-*co*-SMA)) double network hydrogel (LM hydrogel). The synergistic effect of the rigid PVA microcrystal network and the ductile P(AAm-*co*-SMA) hydrophobic network, together with the ionic coordination and hydrogen bonds between polymer networks (multiple physical cross-links), endow the LM hydrogel with excellent super-stretchability (2000%), toughness (3.00 MJ $m^{-3}$), notch resistance, and self-healing property (healing efficiency > 99% at 25 °C after 24 h). The LM hydrogel exhibits sensitive strain sensing behavior, allowing human–computer interaction to achieve motion recognition and health monitoring. Significantly, owing to the excellent photothermal effect and low infrared emissivity of EGaIn, the LM hydrogel reveals great potential in infrared camouflage. The work of self-healing conductive liquid metal hydrogels will promote the research and practical application of hydrogels and liquid metal in intelligent devices and military fields.**

### New concepts

Conductive hydrogels have shown extensive potential in intelligent sensors, electronic skin, wearable devices, and implantable devices. However, it's challenging to achieve a toughness, self-healing, and conductive hydrogel due to the inherent rigidity of the conjugate structure of the conductive polymer and the incompatibility of the conductive fillers with the hydrogel matrix. Herein, gallium indium alloy (EGaIn) microspheres are utilized to construct a super-stretchable and self-healing liquid metal/PVA/P(AAm-*co*-SMA) double network hydrogel. EGaIn microspheres not only act as an initiator to build a ductile P(AAm-*co*-SMA) hydrophobic association network but also yield coordination interactions with PVA microcrystalline network and hydrogen bonds with P(AAm-*co*-SMA) network, leading to multiple physical cross-links within the hydrogel. The achieved hydrogel enables impressive stretchability (2000%), self-healing efficiency (healing efficiency > 99% at 25 °C after 24 h), and sensitivity in strain detection (GF = 7.21, $R^2$ = 0.999), which exceeds that of most reported hydrogels. The hydrogel doesn't only allow for human–computer interaction to achieve motion recognition and convert gestures into numbers but also reveals great potential in infrared camouflage owing to the excellent photothermal effect and low infrared emissivity of EGaIn, sketching a promising future for them in intelligent devices and military fields in modern technologies.

## 1. Introduction

Hydrogels are one kind of soft material with a three-dimensional network structure composed of hydrophilic polymer chains and a large amount of water (50–90%).[1] They have been widely used in waste treatment,[2] agricultural and food chemistry,[3] environmental engineering,[4] medicine,[5] and tissue engineering[6] because of their unique properties such as ionic transmission,[7] stimulus response,[8] low sliding friction[9] and biocompatibility.[10] By introducing ions, conductive polymers, and conductive fillers, hydrogels can achieve electrical conductivity, which enables their implementation in intelligent sensors, electronic skin, wearable devices, and implantable devices.[7] However, due to the inherent rigidity of the conjugate structure of the conductive polymer,[11] the incompatibility of the conductive fillers with the hydrogel matrix,[12] and the salting-out effect,[13] most current conductive hydrogels have poor mechanical properties, *e.g.*, low toughness, low tensile strength, and unsatisfactory self-recovery as well as self-healing properties, which greatly limits the application areas of hydrogels, such as intelligent sensors[14] and electronic skin.[15] The current effective ways to toughen conductive hydrogels are introducing nanofillers[16] and incorporating sacrificial dynamic

[a] *Key Laboratory of Photovoltaic and Energy Conservation Materials, Institute of Solid State Physics, HFIPS, Chinese Academy of Sciences, Hefei 230031, China. E-mail: xzhang@issp.ac.cn*
[b] *University of Science and Technology of China, Hefei 230026, China*
[c] *College of Materials Science and Engineering, Zhengzhou University, Zhengzhou, Henan 450001, China. E-mail: yyyang@zzu.edu.cn*

† Electronic supplementary information (ESI) available. See DOI: https://doi.org/10.1039/d3mh00341h

bonds[17] to achieve effective energy dissipation mechanisms, such as importing hydrophobic associated network[18] and designing double network structure.[19] Shojaei's group[18] developed highly absorbent and tough hydrophobic associated hydrogel utilizing ternary polymerization of polyacrylic acid (PAA), polyacrylamide (PAM) and lauryl methacrylate (LMA) with micelles as physical junctions. Gao's group[17] successfully prepared P(AAm-*co*-LMA) conductive hydrogels with excellent mechanical properties by introducing hybrid latex particles and hydrophobic association. Ran's group[19] mixed PVA and PAAm homogeneously by the one-pot method. The strong hydrogen bond between PVA and PAAm and the microcrystals of PVA after freeze–thawing as sacrificial dynamic bonds successfully toughened the conductive hydrogel and gave the hydrogel excellent self-healing properties.

Gallium indium alloy (EGaIn), as one kind of liquid metal (LM) that has a melting point close to or below room temperature,[20–22] has been widely used in electronic devices, thermal management, soft robots, and biological devices due to its excellent electrical and thermal conductivity,[23,24] low melting point (15.6 °C),[25] and non-toxicity.[26] In addition, EGaIn can be prepared into EGaIn microspheres by ultrasonic dispersion,[27,28] which can be used as nanofillers. EGaIn microsphere fillers are different from other rigid nanofillers because they can adapt to the deformation of the polymer matrix, thus effectively toughening the polymer.[29,30] And the EGaIn microspheres have excellent photothermal properties.[31,32] Meanwhile, the gallium (Ga) in EGaIn is easily oxidized when exposed to air, forming the dense layer of gallium oxide, which has excellent adhesion to most substrates, even those with very low surface energy,[33–35] and $Ga^{3+}$ is able to coordinate with carboxyl and hydroxyl groups to yield sacrificial dynamic bonds for energy dissipation.[36,37] In addition, the gallium (Ga) in EGaIn can initiate the free radical polymerization of vinyl monomer.[38] Therefore, Ga-containing LMs can be filled into polymer matrixes such as polyvinyl alcohol (PVA) and polyamide acid (PAA)[30,39] for achieving high mechanical properties.

Herein, we firstly construct a LM hydrogel (liquid metal/polyvinyl alcohol/*p*(acrylamide-*co*-octadecyl methacrylate) double network hydrogel) integrated with functions of human–computer interaction and infrared camouflage *via* simply one pot method, wherein the EGaIn microspheres can act as not only initiators to induce the copolymerization of AAm and SMA to fabricate P(AAm-*co*-SMA) hydrophobic associated network, but also as flexible nanofillers to toughen the hydrogel. The hydroxyl groups of PVA chains can coordinate with $Ga^{3+}$ of EGaIn microspheres to form physical cross-link, and then freeze–thaw cycle is performed to enhance the hydrogen bonding within PVA chains to yield rigid microcrystalline network.[40] The P(AAm-*co*-SMA) chains grow from the surface of EGaIn microspheres, wherein the hydrophobic SMA segments are inside the micelles. Intermolecular hydrogen bonds can be formed between the PVA network and P(AAm-*co*-SMA) network, and EGaIn microspheres can also generate physical interactions with the dual networks, improving the compatibility of the two networks. Overall, LM hydrogel with multiple physical cross-links not only can dissipate massive energy to toughen the hydrogel, but also possesses outstanding self-healing properties due to the reversibility and rebuildability of physical cross-links. LM hydrogel exhibits excellent elasticity, super-stretchability, toughness, notch resistance, and moderate mechanical strength similar to human skin. Additionally, owing to the distinct combination of excellent mechanical flexibility and conductivity, the LM hydrogel reveals sensitive strain and pressure sensing performance to achieve human motion recognition and human–computer interaction. Furthermore, LM hydrogel possesses excellent photothermal properties due to the EGaIn microspheres, and the LM coating provides the hydrogels with low infrared emissivity. The multifunctional LM hydrogel is expected to be applied in the fields of human–computer interaction and infrared camouflage.

## 2. Results and discussion

### 2.1. Preparation and structure of LM hydrogel

The preparation method of LM hydrogel is shown in Fig. S1 (ESI†). The EGaIn is added to a 10 mL SDS/NaCl aqueous solution and then ultrasonically dispersed for 15 min to obtain the EGaIn microsphere suspension, which has an average particle size of 183.9 nm, as shown in Fig. S2 (ESI†). Afterward, the EGaIn microsphere suspension is added to the hydrogel solution consisting of AAm, SMA, and PVA. The mixture is stirred and pre-cured at 45 °C for 15 min. It is then poured into the mold for curing for 24 h, followed by two freeze–thaw cycles, and LM hydrogel-*n* (*n* denotes the mass ratio of EGaIn to PVA) is obtained.

Gallium can initiate free radical polymerization of vinyl monomers;[38,41] as shown in Fig. 1f, the C=C infrared absorption peak[38,42] at 1608 $cm^{-1}$ in LM hydrogel is significantly lower, and the whole infrared absorption spectrum is similar to that of the photo-initiated hydrogel. In addition, the XPS spectra of the LM hydrogel and the photo-initiated hydrogel show little C=C content at 284.4 eV,[43] which are also similar (Fig. 1d). These prove the successful polymerization of LM hydrogel. Herein, many P(AAm-*co*-SMA) polymer chains grow from the LM microspheres at the same time, and Ga and P(AAm-*co*-SMA) polymer chains are chemically linked,[38] so that the LM microspheres can be seen as "chemical cross-links" (Fig. 1a and Fig. S3b, ESI†). As shown in Fig. S4 (ESI†), the LM microspheres and the connected polymer chains occur slippage upon external mechanical deformation or pressure, benefiting the stretchability of LM hydrogels. The micelles act as physical junctions in the P(AAm-*co*-SMA) can be destroyed for dissipating energy and enhancing the mechanical performance of LM hydrogel.

In addition, $Ga_2O_3$ on the surface of EGaIn microspheres interacts with the hydroxyl group in PVA chains.[36,37] As shown in Fig. 1e, the hydroxyl group infrared absorption peak of LM/PVA hydrogel shifts from 3307 $cm^{-1}$ to 3273 $cm^{-1}$, compared with pure PVA hydrogel. To demonstrate the interaction between EGaIn microspheres and PVA more intuitively, experiments are designed to compare the settling rate of EGaIn microspheres in aqueous PVA solutions and pure water. As shown

 

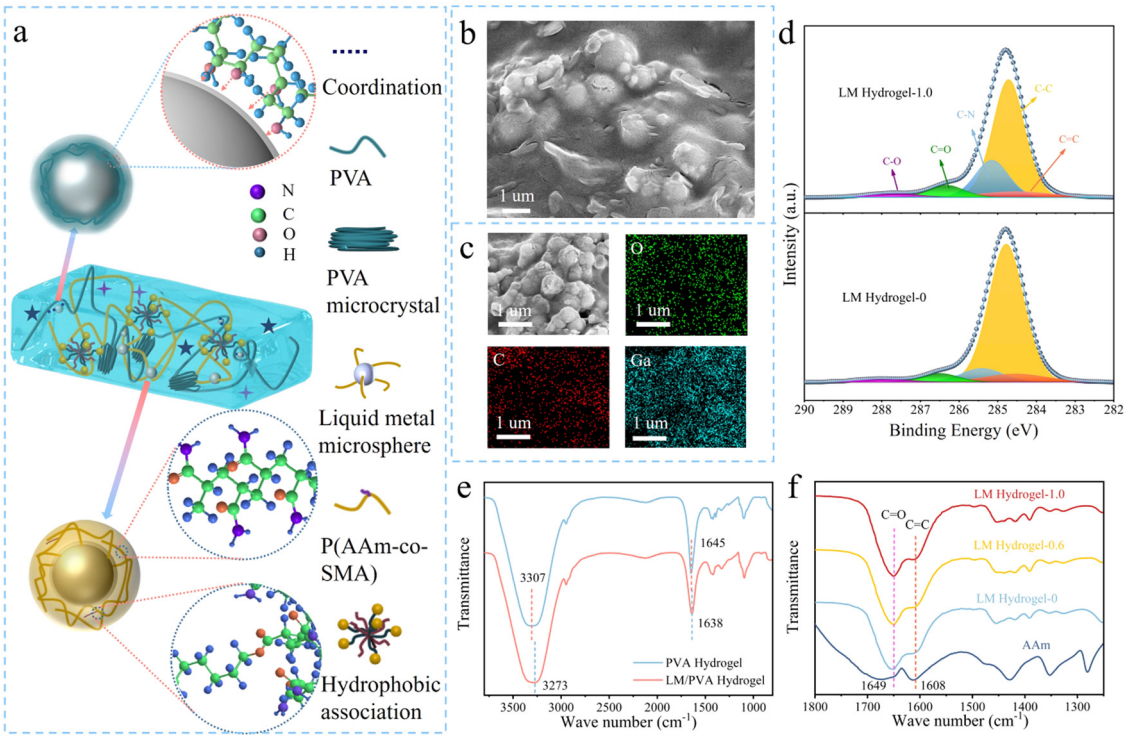


Fig. 1 (a) Schematic diagram of the structure of LM hydrogel. PVA coordinately wraps the EGaIn microspheres, and P(AAm-*co*-SMA) molecular chains grow on the surface of the EGaIn microspheres. (b) EGaIn microspheres are encapsulated by PVA, P(AAm-*co*-SMA) molecular chains and present in the hydrogel matrix. (c) The SEM image and EDS spectrum (EDS mapping) of LM hydrogel. (d) Comparison of XPS images of LM hydrogel-0 and LM hydrogel-1.0. (e) FT-IR spectra of PVA hydrogel and LM hydrogel. (f) FT-IR spectra of LM hydrogel-0, LM hydrogel-0.6, LM hydrogel-1.0, and AAm.

in Fig. S5 (ESI†), EGaIn microspheres precipitate in deionized water after 8 h, while they remain uniformly dispersed in a PVA aqueous solution even after 72 h, proving the interaction between PVA chains and EGaIn microspheres. Therefore, LM microspheres can promote the yield of PVA crosslinked network *via* the ligand complexation and hydrogen bonding between PVA chains and LM microspheres, as shown in Fig. 1a and Fig. S3a (ESI†). In addition, the freeze-thaw cycle of LM hydrogel can lead to the formation of microcrystals in the PVA of the LM hydrogel, as shown in Fig. S6 (ESI†). These microcrystals also act as physical cross-links in the PVA network.

In this work, the LM microspheres not only bind with the PVA chain to form a weak PVA network with low water absorption ability but also induce polymerization of AAm and SMA to generate a P(AAm-*co*-SMA) network with high water absorption ability. The content of LM microspheres substantially affects the polymerization rate and the formation of the P(AAm-*co*-SMA) network, which determines the final state of hydrogel system. As the concentration of LM microspheres is low, the LM microspheres preferentially bind with PVA chains rather than induce polymerization, and the polymerization rate is too slow to generate a P(AAm-*co*-SMA) network. As shown in Fig. S7 and S8 (ESI†), when the ratio of LM to PVA is 0.2 : 1.0, the LM microspheres bind with PVA chains into a low-water-content hydrogel that precipitates from the aqueous solution, and the P(AAm-*co*-SMA) network was not successfully yielded. When the concentration of LM microspheres is high, the polymerization rate is fast, and the P(AAm-*co*-SMA) network can be generated while forming a PVA network, resulting in a double-network LM hydrogel.

For LM hydrogel, the intermolecular hydrogen bonds can be formed between the PVA network and P(AAm-*co*-SMA) network, and EGaIn microspheres can also generate physical interactions with the dual networks, benefiting the compatibility of the two networks. SEM images of LM hydrogel further demonstrate this; as shown in Fig. 1b, c and Fig. S9 (ESI†), EGaIn microspheres are encapsulated with polymer, while the two networks are integrated and cannot be distinguished. Due to the excellent interaction between the EGaIn microspheres and the hydrogel matrix, the flowing EGaIn microspheres are well encapsulated in the hydrogel matrix, avoiding the leakage of EGaIn microspheres under severe pressing and twisting, as shown in Fig. S10 (ESI†).

### 2.2. Mechanical properties of LM hydrogel

As shown in Fig. 2a, LM hydrogel-1.0 can be easily stretched more than 10 times, even under twisting and knotting. In addition, LM hydrogel has excellent toughness, as shown in Fig. 2c. LM hydrogel is not damaged when pressed by a sharp surgical blade, and it recovers quickly after the blade is removed. The stress–strain curve of LM hydrogel (Fig. 2d) shows that the EGaIn microspheres decreased Young's modulus and fracture strength of the hydrogel compared with the photoinitiated PVA/P(AAm-*co*-SMA) double network hydrogel, but the EGaIn microspheres increased the elongation at break

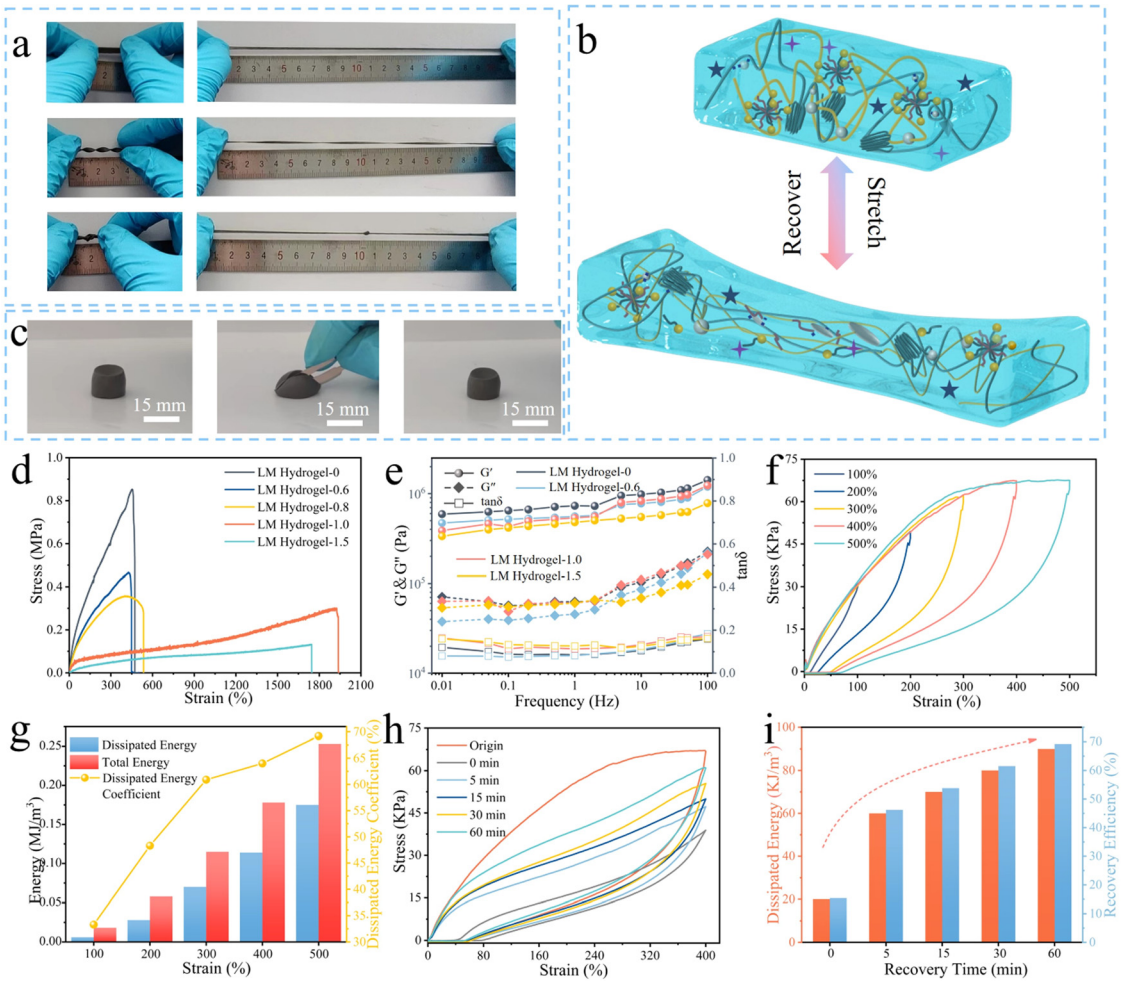


Fig. 2 (a) LM hydrogel-1.0 can be easily stretched more than 10 times, even under twisting and knotting. (b) A schematic representation of the destruction and reformation of the LM hydrogel's physical cross-links and the deformation and recovery of the LM microspheres. (c) LM hydrogel-1.0 is not damaged when pressed by a sharp surgical blade, and it recovers quickly after the blade is removed. (d) Stress–strain curves for LM hydrogel-*n* (*n* = 0, 0.6, 0.8, 1.0, and 1.5). (e) Curves of storage modulus, loss modulus, and loss tangent angle of LM hydrogel-*n* (*n* = 0, 0.6, 1.0, and 1.5) as a function of load frequency. (f) Loading–unloading curves of LM hydrogel-1.0 at strains of 100%, 200%, 300%, 400%, and 500%. (g) Dissipative energy, total energy, and dissipative energy efficiency of LM hydrogel-1.0 stretching at 100%, 200%, 300%, 400%, and 500%. (h) Loading–unloading curves of LM hydrogel-1.0 stretched 400% and then recovered for 0, 5, 15, 30, and 60 min. (i) Dissipation energy and recovery efficiency of LM hydrogel-1.0 stretched 400% and then recovered for 0, 5, 15, 30, and 60 min.

of the double network hydrogel. The content of LM microspheres affects the physical cross-linkers of PVA network. With the increase of the content of LM microspheres, the physical interactions between LM microspheres and PVA chains enhances, and the microcrystalline zones of PVA network decrease, resulting in a reduction of rigidity of the PVA microcrystalline network. As shown in Fig. S6 (ESI†), the crystallization peaks of LM/PVA hydrogels are significantly lower than that of pure PVA hydrogel, and the crystallization peaks of LM hydrogels-*n* (*n* = 0.6, 0.8, 1.0, and 1.5) are significantly lower than that of LM hydrogel-0. The elastic modulus and fracture strength of LM hydrogels mainly are determined by the rigid PVA network. So, the elastic modulus and fracture strength of LM hydrogels gradually decrease with the increase in the content of LM microspheres.

Unlike most rigid nanoparticles that reinforce the rigidity of hydrogel,[29,30,41] the LM microspheres in this study serve as flexible and fluid fillers to toughen the LM hydrogel. Upon deformation, the LM microspheres and the connected polymer chains occur slippage, resulting in an improvement in the stretchability and toughness of the LM hydrogel. As shown in Fig. 2d and Fig. S11a (ESI†), the stretchability and toughness of LM hydrogels significantly improve as the ratio of LM to PVA increases from 0.6 to 1.0. However, as the ratio of LM to PVA increases to 1.5, although the fracture strain achieves a high value of 1700%, the low mechanical strength leads to a low toughness value (Fig. 2d and Fig. S11a, ESI†). Besides, when the ratio of LM to PVA is higher than 1.5 (for example, 2.0), the obtained LM hydrogel is very soft, like chewing gum or plasticine (Fig. S12c, ESI†). In summary, when the LM to PVA mass ratio is 1.0, the LM hydrogel shows optimal mechanical properties with an elongation at a break of 2000%, a fracture strength of 0.30 MPa, and a toughness area of 3.00 MJ $m^{-3}$

 

(if not stated otherwise, the LM hydrogel-1.0 is used for the next characterization and tests).

Upon external force, the physical cross-links of LM hydrogel are destroyed and the EGaIn microspheres occur deformation for dissipating energy (Fig. 2b, f and g). After the external force is removed, the physical cross-links are reconstructed and the EGaIn microspheres recover the original shape. As the strain increases, the area of the dissipative ring gradually increases, and the percentage of dissipated energy gradually increases, reaching 70% when the strain reaches 500%. Besides, the LM hydrogel was cycled 10 times at 400% strain, as shown in Fig. S11d (ESI†). During the continuously multiply loading–unloading cycles, compared with the first loading–unloading cycle, the hysteresis loop and corresponding dissipated energy of the second cycle sharply decrease to 21.9%, meaning that most physical cross-linkers in LM hydrogel are destroyed in the first cycle and cannot be recovered instantly and completely. The destroyed microcrystalline zones and micelles cannot be quickly recovered, while the dissociated hydrogen bonding interactions in hydrogels can be healed promptly. Therefore, during the subsequent cycles, especially in 6–10th cycles, the dissipated energy slightly decreases and the hysteresis loops are almost overlapped, together with the almost stable maximum loading force. Similarly, the physical cross-links can be reformed and the EGaIn microspheres can recover, so LM hydrogels have excellent self-recovery properties. The first stretch breaks most of the physical interactions in the hydrogel, and the recovery efficiency of the hydrogel reaches 70% when the stretched LM hydrogel is released and kept at room temperature for 60 min, as shown in Fig. 2h and i. In addition, continuous 50 elongation-relaxation cycles are performed to investigate the mechanical durability of the as-prepared LM hydrogel. As shown in Fig. S11b and c (ESI†), during the continuous 50 cycles, there is a sharp drop for hysteresis value of the LM hydrogel after the first cycle and the maximum loading force and hysteresis loop in 5–50th cycles remain stable, demonstrating the general mechanical durability of the LM hydrogel.

Besides, LM hydrogels have excellent compressibility; as shown in Fig. S11e (ESI†), LM hydrogels are compressed by 75% without fracture. LM hydrogels also have excellent compressibility stability, as shown in Fig. S9f (ESI†), where the LM hydrogels are easily reciprocated 50 times at 30% strain. Then, rheological tests are performed on LM hydrogels. As shown in Fig. 2e, with the increase of LM content, the storage modulus decreases gradually, but the loss modulus decreases and then increases. When compared to the PVA/P(AAm-*co*-SMA) double network hydrogel, the loss tangent angle of the LM hydrogel does not change much, while the loss tangent angle of the LM hydrogel-0.6 decreases, indicating that while EGaIn is flexible, the EGaIn microspheres increase the cross-links without destroying the hydrogel's elasticity.

### 2.3. Notch resistance, self-healing properties, and adhesion properties of LM hydrogel

LM hydrogel has outstanding notch resistance because of the multiply physical cross-linkers structure. The LM hydrogel-1.0 strip with a notch of 1/3 width (Fig. S14, ESI†) can still be stretched to 800%, while the notched PVA/P(AAm-*co*-SMA) double network hydrogel can only be stretched to 240% (Fig. 3a). As shown in Fig. 3b and Movie S1 (ESI†), when the strain of the LM hydrogel-1.0 strip is at 500%, the strain at the notch has reached 1800%. Furthermore, notched LM hydrogel-1.0 can be sustained 50 loading–unloading cycles at the strain of 200%, as shown in Fig. S15a (ESI†). During the continuous 50 cycles with a maximum strain of 200%, the notch of the LM hydrogel remains semicircular and grows slowly, which is ascribed to the effective energy dissipation mechanism provided by multiple physical cross-linkers in the LM hydrogel. Significantly, the semicircular shape rather than the triangular shape of the notch clearly demonstrates that the LM hydrogel is notch blunting. In addition, after 50 cycles, although the structure at the hydrogel notch is destroyed (Fig. S15c and d, ESI†), the generated filamentous connection still connects the two ends of the notch to prevent further growth of the notch (Fig. S15b, ESI†), indicating the excellent notch resistance in multiple consecutive cycles.

The multiple physical cross-links and fusionable EGaIn microspheres endow the LM hydrogel with excellent self-healing properties in addition to excellent toughness and self-recovery properties. When the cut LM hydrogel contact again, the interfacially physical cross-links such as hydrophobic association, hydrogen bonding, and interaction between PVA chains and gallium oxide can be rebuilt, and the scattered EGaIn microspheres in interface can be integrated (Fig. 3h). As shown in Fig. 3d, LM hydrogel-1.0 gradually heals at room temperature, and the healing efficiency of breaking strength and elongation at break reached 99% after 24 h (Fig. 3g). And the location of the breakage again is not at the healing wound, as shown in Fig. 3e, proving that LM hydrogel has excellent self-healing properties. Similarly, since LM hydrogels are multiple physically cross-linked hydrogels, they are recyclable and can be dissolved in water at high temperatures for remolding (Fig. S16, ESI†). Meanwhile, the conductive properties of LM hydrogel can be self-healed. As shown in Fig. 3f, the cut LM hydrogel is put in contact, and the current immediately returns to more than 99% of the initial current (Fig. 3g).

Besides, LM hydrogel also has excellent adhesion properties due to the excellent adhesion properties of PVA[44–46] and $Ga_2O_3$. As shown in Fig. S17a–h (ESI†), LM hydrogel can adhere to copper, stainless steel, glass, plastic, wood, rubber, and other materials. And LM hydrogel has better adhesion to wood and paper (Fig. S17j, ESI†). A 90° peeling test of the hydrogel and the wood board clearly shows the LM hydrogel that has been deformed by adhesion and pulling (Fig. S17i, ESI†).

### 2.4. Sensing performance and human–computer interaction of LM hydrogel

LM hydrogel is rich in ions, such as $Cl^-$ and $Na^+$, which grant it excellent conductivity. The small light bulb connected in the circuit with LM hydrogel continues to glow, as shown in Fig. 4a. The conductivity of LM hydrogel is measured to be 0.55 S $m^{-1}$ (Fig. 4b), and the conductivity of LM hydrogel has little

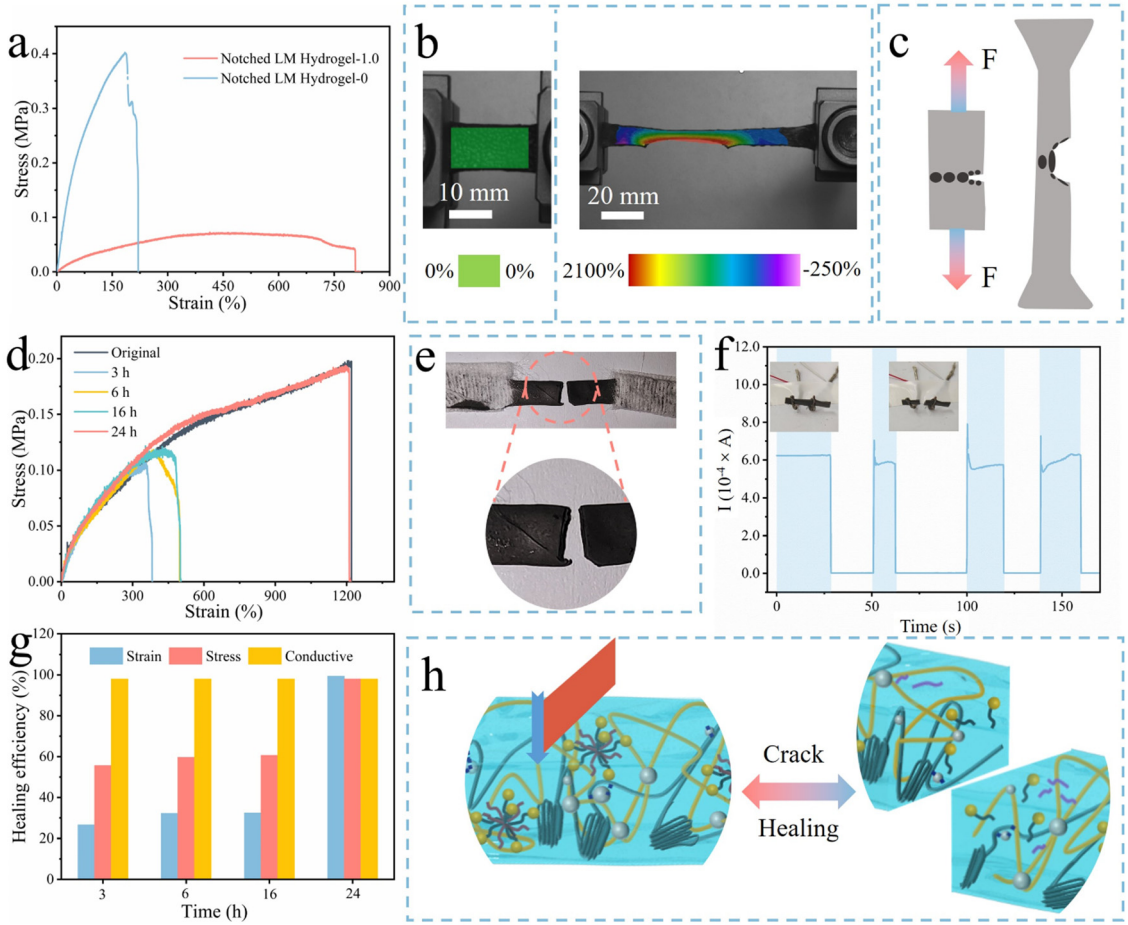


Fig. 3 (a) Stress–strain curves of notched LM hydrogel-0 and notched LM hydrogel-1.0. (b) Diagram of the LM hydrogel before and after stretching with a notch. (c) A schematic diagram of the mechanism of LM hydrogel's notch resistance. (d) Comparison of stress-strain curves of LM hydrogel after 3, 6, 16, and 24 h of healing and the initial LM hydrogel. (e) The healed LM hydrogel was not broken at the healing areas after stretching again. (f) The conductive self-healing properties of LM hydrogels. The current of LM hydrogel is 0 after cutting, and the current of LM hydrogel recovers after contact. (g) Self-healing efficiency of stress, strain, and conductivity of LM hydrogels at 3, 6, 16, and 24 h. (h) LM hydrogel self-healing mechanism diagram.

relationship with the content of LM, which is because the EGaIn microspheres are encapsulated by the polymer and cannot form the conductive pathway in the matrix, and LM hydrogel mainly relies on the anions and cations in the matrix for conductivity. In addition, the brightness of the small bulb connected to the circuit changed significantly during the stretching process, as shown in Fig. 4a, indicating that the resistance of LM hydrogel changed. Then, the gauge factor (GF) of LM hydrogel is tested; as shown in Fig. S18 (ESI†), the GF of LM hydrogel-1.0 is more prominent, which may be related to the shape change of the hydrogel matrix and EGaIn microspheres during the stretching process. The GF value of LM hydrogel-1.0 is about 3.42 in the strain range of 0–500%, and the GF value reaches 7.21 after the strain exceeds 500%, as shown in Fig. 4c, which is superior to most of reported hydrogel sensors[30,41,47–66] (Fig. 4f).

In addition, the resistance change ($\Delta R/R_0$) of LM hydrogel-1.0 is tested under small and large strains, as shown in Fig. 4d. LM hydrogel's resistance changes with increasing strain with a distinct change, indicating that LM hydrogel has the potential for human–computer interaction systems such as strain sensors and pressure sensors. The conductivity and resistance change of the LM hydrogel remain stable after 200 cycles at 200% strain, as shown in Fig. 4e. Therefore, the strain sensors prepared by LM hydrogel will have excellent conductivity stability and long service life. LM hydrogel-1.0 also shows a notable sensitivity to compression, as shown in Fig. 4g, the GF remains at 0.70 even at strains lower than 50%. In addition, the compressive stress sensitivity of LM hydrogel-1.0 is analyzed and shown in Fig. 4h. The LM hydrogel-1.0 shows sensitivities of 19.94 $MPa^{-1}$, 7.85 $MPa^{-1}$, and 3.92 $MPa^{-1}$ for the three stages of 0–0.038 MPa, 0.038–0.14 MPa, and 0.14–0.20 MPa, respectively. Moreover, LM hydrogel-1.0 maintains relatively stable electrical conductivity under different compressive strains (stresses), as shown in Fig. 4i. The high conductivity and large GF grant LM hydrogels great potential to be used as pressure sensors.

LM hydrogel easily loses water in the air, which makes it difficult to use for a long time. In this experiment, a strain sensor was prepared by encapsulating LM hydrogel with 3 M tape, as shown in Fig. S19 (ESI†). The LM hydrogel strain sensor

 

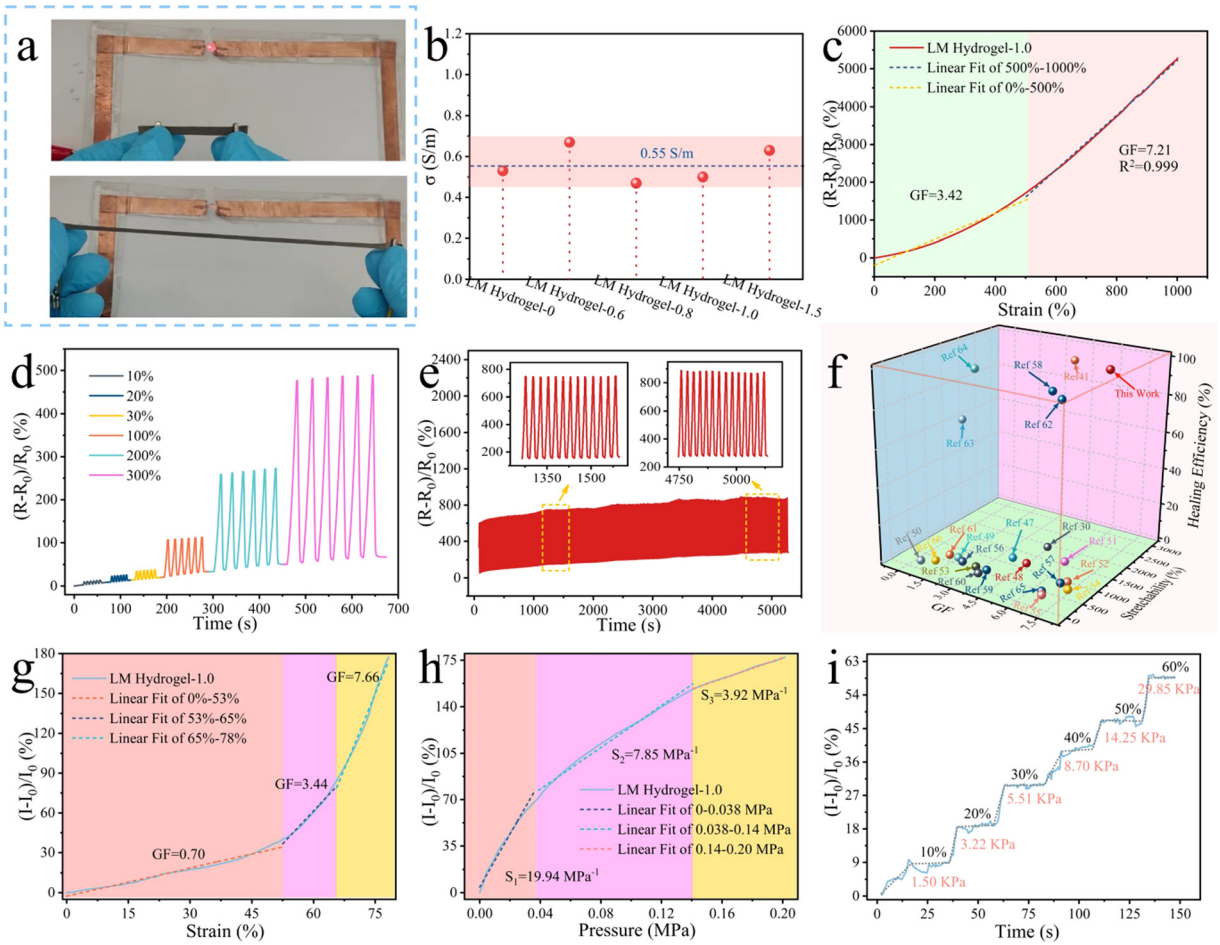


Fig. 4 (a) The LM hydrogel-1.0 is used as a wire, and the bulb is lit. When the hydrogel is stretched, the bulb is dimmed. (b) The conductivity of LM hydrogels with different LM contents is all in the range of 0.55 S $m^{-1}$. (c) The GF of LM hydrogel-1.0 under different strains. (d) The resistance changes of LM hydrogel-1.0 at 10%, 20%, 30%, 100%, 200%, and 300% strains for six repetitions. (e) The resistance changes of LM hydrogel-1.0 at 200% strain in 200 successive cycles. (f) The GF, self-healing efficiency, and stretchability of LM hydrogels exceed those of most reported hydrogels. (g) The GF of LM hydrogel-1.0 in pressure. (h) The pressure sensitivity of LM hydrogel-1.0. (i) The rate of change of current in LM hydrogels under different pressures.

can detect human body movements *via* transforming the motion into electrical signal. As shown in Fig. 5a, the strain sensor is attached to the finger to monitor the bending angle of the finger. The rate at which the resistance changes on the strain sensor follows the bending of the finger at 30°, 60°, and 90°. The sensor monitors the bending of the arm by attaching the strain sensor to the arm joint. As the bending angle of the arm increases, the rate of resistance change of the sensor gradually increases. The strain sensor is attached to the knee to monitor the body's activity. As shown in Fig. 5c, walking has a slower bending frequency and greater movement of the leg compared to running, so the current signal changes more slowly and with greater variation for walking. Jumping 30 cm requires a higher knee bending angle than jumping 10 cm, and landing requires knee bending to cushion. The LM hydrogel sensor can monitor and distinguish the two kinds of jumps, as shown in Fig. 5d. Attaching the strain sensor at the throat can monitor the actions of nodding, shaking the head, and drinking, as shown in Fig. 5e and f. The hydrogel sensor can accurately monitor and capture swallowing when drinking water. By attaching the strain sensor to the forehead, the sensor can monitor changes in human expression, *e.g.*, the frowning action, as shown in Fig. 5g. More importantly, strain sensors attached to the face can monitor the movement of human speech. As in Fig. 5h, the movement of the volunteer saying each letter is unique, and so are the corresponding current changes. In addition to individual letters, the facial movements of the experimental volunteer during simple conversations, such as "How are you?" and "I'm fine." can also be accurately captured.

As shown in Fig. 6a and Fig. S20 (ESI†), LM hydrogel can also be prepared as a pressure sensor by directly encapsulating it in silicone rubber with leads connected at both ends. The pressure sensor can accurately monitor the pressure change when writing different letters such as "CAS" and "USTC", as shown in Fig. 6b and c. Compared to various human motions, the writing behaviors are very subtle and local area of LM hydrogel is stimulated by external forces, producing relatively small

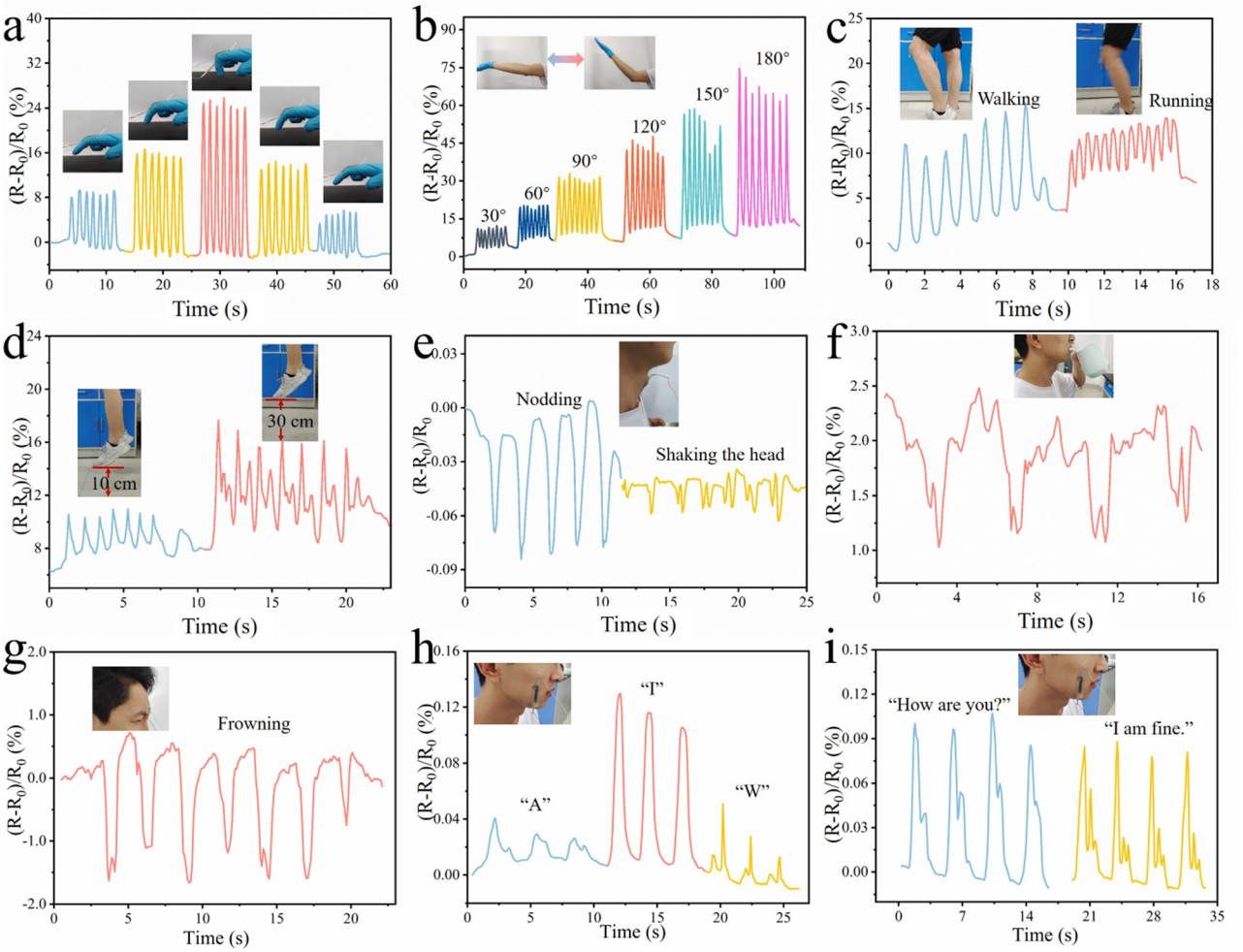


Fig. 5 Motion detection: (a) the finger bending angle, (b) the arm bending angle, (c) movement characteristics during walking and running, (d) movement characteristics when jumping different heights, (e) head nodding and head shaking, (f) drinking water, (g) frowning, (h) the vocalization of different letters, and (i) vocalization during simple communication.

changes in resistance. By detecting the subtle changes in electrical signal and comparing the pressure changes when writing different letters, the content of the subject's writing can be recognized.

Furthermore, LM hydrogel strips are attached to the glove's five fingers and connected to the wires for preparing functional glove, enabling human–computer interaction *via* detecting the finger bending (Fig. 6d and e). After the experimental volunteers put on the glove, they can output the desired numbers on the LCD by bending and extending their fingers. As shown in Fig. 6f and Movie S2 (ESI†), the LCD shows 5 when the experimental volunteer extends five fingers and 0 when the experimental volunteer makes a fist. What's more, the human–computer interaction glove is universal, and other experimental volunteers wearing the glove can also achieve human–computer interaction, as shown in Movie S3 (ESI†).

### 2.5. Infrared camouflage property

EGaIn microspheres have excellent infrared absorption and photothermal properties, and the smaller the microsphere size, the better the photothermal performance.[39,67] When the 808 nm near-infrared laser (NIR) of 1.5 W cm$^{-2}$ is irradiated on LM hydrogel (Fig. 7a), EGaIn microspheres can convert the light energy into heat energy, rendering the gradual increase of temperature from 28 °C to 71 °C in 1 min (Fig. 7b). And with the increase in laser power, the heating rate of LM hydrogel becomes faster, as shown in Fig. 7c. The higher the laser power, the higher the temperature of the hydrogel after heating for 1 min (Fig. 7d). In addition, the photothermal properties of LM hydrogel have good stability; as shown in Fig. 7e, the hydrogel is subjected to heating for 30 s and cooling for 150 s cycle experiment under the 808 nm NIR at 1.25 W cm$^{-2}$, and the hydrogel does not change its temperature greatly due to low water content (<20%) while sacrificing the mechanical properties, self-healing properties, and electrical conductivity. Therefore, LM hydrogel has the potential for dynamic infrared camouflage in varied background. As shown in Fig. 7f, a piece of LM hydrogel film is attached to a toy piglet to investigate the capacity of infrared camouflage over broad temperature range of 25–65 °C. When the background temperature changes,

 

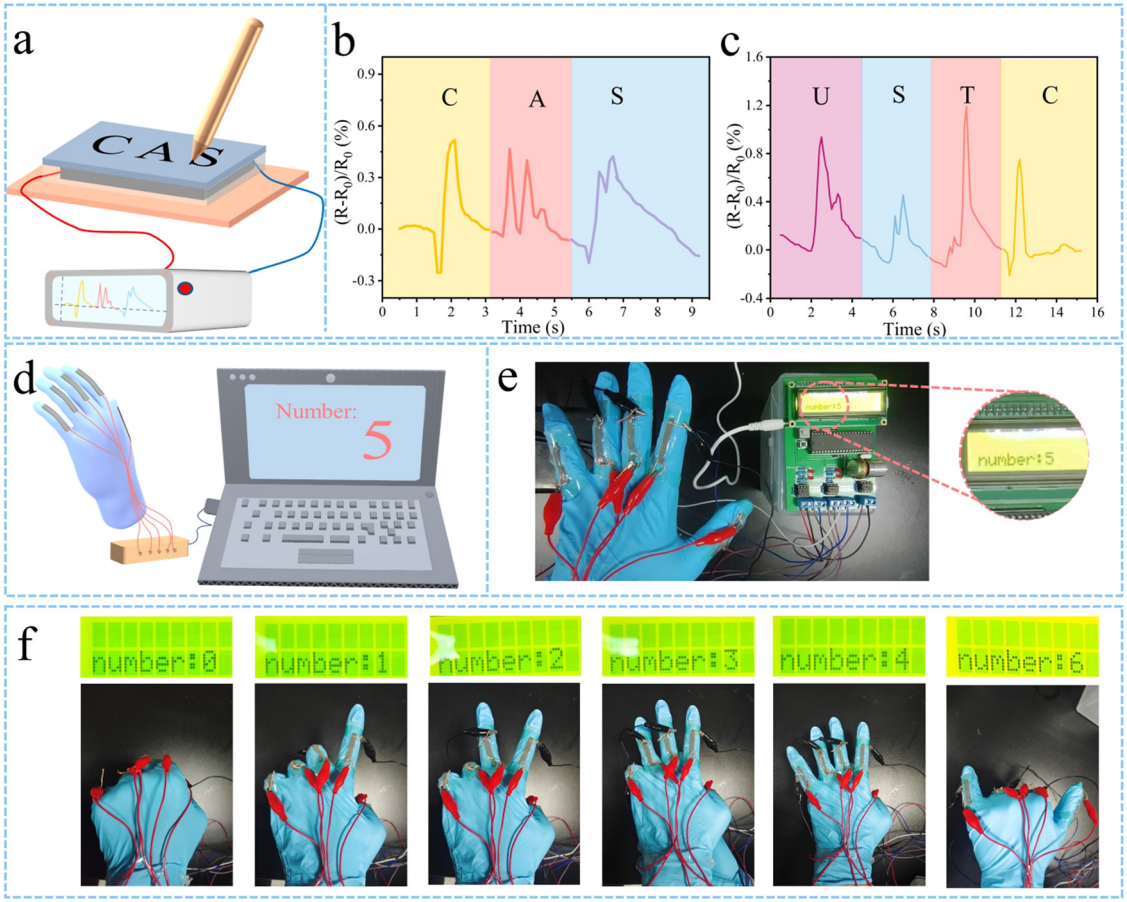


Fig. 6 (a) A schematic diagram of the pressure sensor. (b and c) The resistance changes when writing "CAS" and "USTC" on the pressure sensor. (d) A schematic diagram of the human–computer interaction system. (e) The volunteer wearing the human–computer interaction glove opens his finger, and the LED screen displays the number "5". (f) The human–computer interaction glove prepared by LM hydrogel displays numbers according to the bending of the volunteer's finger.

dynamic infrared camouflage can be achieved by controlling the intensity and the illumination time of the laser to make the hydrogel temperature consistent with the background temperature. Meanwhile, a fighter jet model coated with LM hydrogel film cannot be observed *via* infrared camera and realize dynamic infrared camouflage (Fig. S21, ESI†).

What's more, bulk EGaIn or EGaIn coating is similar to metals such as silver and has an extremely strong reflectivity of light, including the infrared band; that is, EGaIn coating has a low emissivity in the infrared band (Fig. S22a, ESI†). Therefore, coating LM hydrogel with a layer of EGaIn (Fig. S22b and c, ESI†) gives the hydrogel excellent static infrared camouflage properties. The LM hydrogel coated with EGaIn refers to infrared camouflaged LM hydrogel. As shown in Fig. 7g, the infrared camouflaged LM hydrogel film and control group are heated on a hot table at 30, 45, and 60 °C. Remarkably, the control group can be easily detected *via* infrared thermography due to the increased temperature, while the infrared camouflaged LM hydrogel film cannot be observed due to low infrared emissivity, indicating excellent infrared camouflage. When it is applied to the fingers and the back of the hand (Fig. S23, ESI†), the infrared thermography also does not detect a significant temperature change and thus achieves static infrared camouflage.

## 3. Experimental section

### 3.1. Materials

EGaIn, consisting of 24.5% In and 75.5% Ga by weight, was purchased from Northeast Nonferrous Metals. Polyvinyl alcohol (PVA), AR 1799, was purchased from Shanghai Titian Scientific Co., Ltd. Acrylamide (AAm), AR 99%, was purchased from Shanghai Aladdin Biochemical Technology Co., Ltd. Sodium dodecyl sulfate (SDS) was purchased from Shanghai Aladdin Biochemical Technology Co., Ltd. Sodium chloride (NaCl) was purchased from Shanghai Aladdin Biochemical Technology Co., Ltd. 2-Hydroxy-4′-(2-hydroxyethyl)-2-methylpropiophenone (photo-initiator, 98%) was purchased from Shanghai Titian Scientific Co., Ltd. Octadecyl methacrylate (SMA), 96%, was purchased from Shanghai Bide Pharmaceutical Technology Co., Ltd. Pure water is prepared by this laboratory. Polydimethylsiloxane (PDMS, Dow Corning SYLGARD 184 Silicone Rubber).

All experiments sought the unity of volunteers and did not cause harm to volunteers.

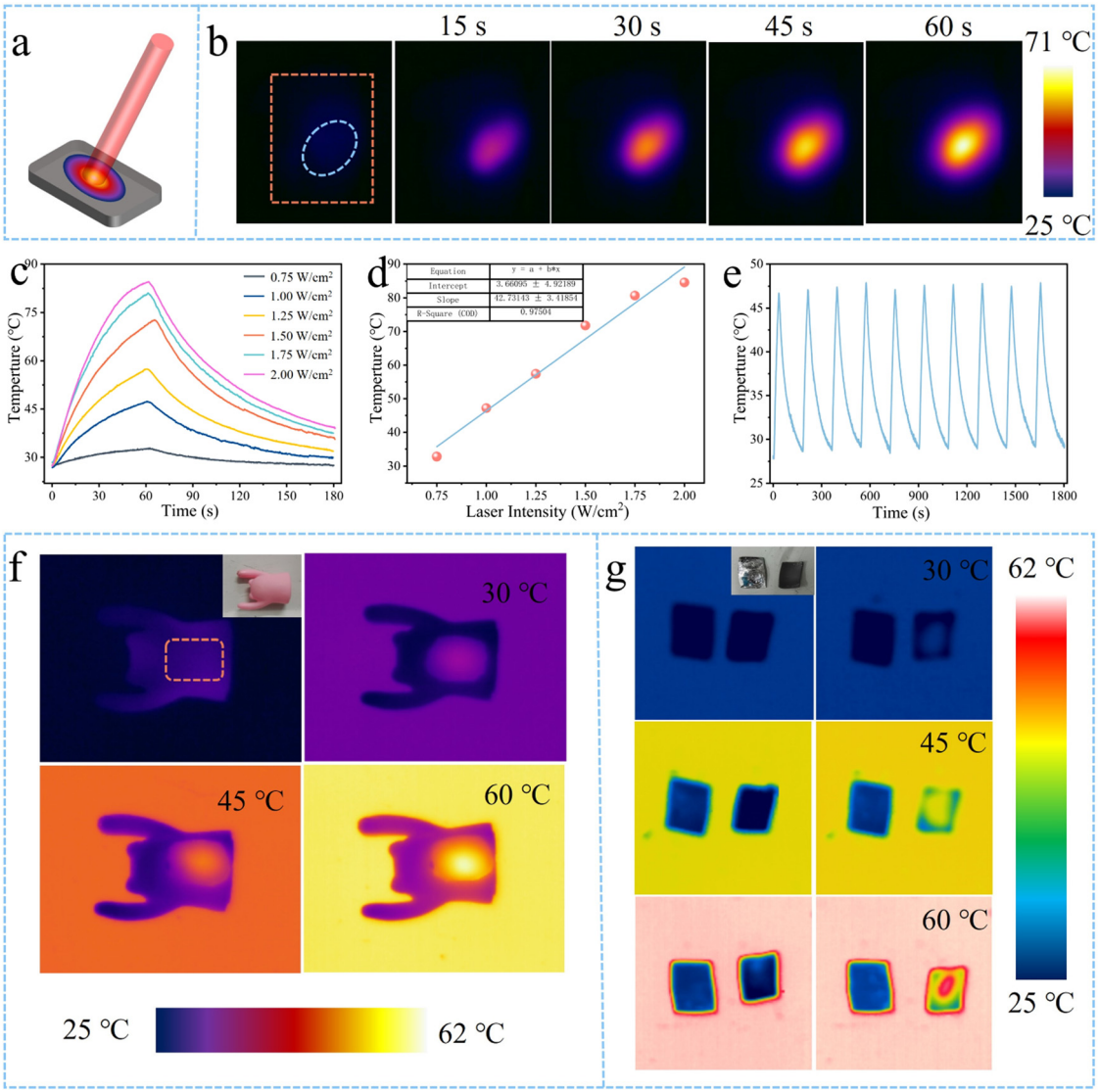


Fig. 7 (a) Schematic diagram of LM hydrogel film under 808 nm near-infrared laser (NIR) irradiation. (b) The temperature variation of the LM hydrogel film under 808 nm NIR irradiation. (c) The temperature change curves of LM hydrogel films at different laser intensities. (d) The temperature of the LM hydrogel film after 60 s of 808 nm NIR irradiation in response to the laser power. (e) Photothermal stability of LM hydrogel films. (f) The dynamic infrared camouflage capability of LM hydrogel films. (g) The static infrared camouflage capability of LM hydrogel films with LM surface coatings.

### 3.2. Preparation of LM hydrogel

**3.2.1. Preparation of SDS/NaCl aqueous solution.** A NaCl aqueous solution was prepared by dissolving 5.845 g of NaCl in 200 mL of pure water. Then 16.00 g of SDS was added to the NaCl aqueous solution, followed by stirring and dissolving at 45 °C in a collector-type constant temperature heating magnetic stirrer (DF-101S Gongyi Yuhua Co., Ltd) for 1 h to obtain SDS/NaCl aqueous solution.

**3.2.2. Preparation of 10 wt% PVA aqueous solution.** 11.11 g of PVA powder was added to 100 g of pure water, followed by stirring at 65 °C for 1 h and 95 °C for another 2 h to obtain a PVA aqueous solution of 10 wt%.

**3.2.3. Preparation of LM hydrogel-0.** SDS/NaCl aqueous solution (10 mL), AAm (2.8636 g), SMA (0.1364 g), and photoinitiator (0.0913 g) were added to the above PVA aqueous solution (5.7250 g, 10 wt%). After stirring for 30 min at 45 °C, the hydrogel solution was poured into the mold and cured under 395 nm UV light (1 kW Baoding Lingwei Electromechanical) for 30 min, followed by two freeze (21 h, −15 °C) and thaw (3 h, 30 °C) cycles to get LM hydrogel-0.

**3.2.4. Preparation of LM hydrogel-*n*.** EGaIn (0.3434 g, 0.4580 g, 0.5725 g, or 0.8586 g) in an SDS/NaCl aqueous solution was sonicated for 15 minutes in an ultrasonic crusher (UX-300, Mitsui Electric Japan) with a power of 75 W in an ice bath to obtain EGaIn microspheres.[28] PVA aqueous solution (5.7250 g, 10 wt%), AAm (2.8636 g), and SMA (0.1364 g) were added to the above EGaIn microspheres-containing SDS/NaCl aqueous solution and kept stirring for 30 minutes at 45 °C. Afterward, the mixture was pre-cured for 15 minutes at 45 °C and then poured into the mold, followed by curing for 24 hours

 

in a constant temperature and humidity chamber (WHTH-80-70-80, Hong Kong Weihuang Technology Co., Ltd) at 98% humidity and 30 °C. After two freeze (21 h, −15 °C) and thaw (3 h, 30 °C) cycles, LM hydrogel-*n* (*n* = 0.6, 0.8, 1.0, and 1.5) was obtained, where n denotes the mass ratio of EGaIn to PVA.

### 3.3. Characterization of LM hydrogel

**3.3.1. Structural analysis of LM hydrogel.** LM hydrogel was freeze-dried by using a freeze dryer (LGJ-10, Beijing Songyuan Huaxing Technology Development Co., Ltd) and then observed by a field emission scanning electron microscope (SU8020, Hitachi). X-Ray photoelectron spectroscopy (XPS) was performed on the hydrogels by using an X-ray photoelectron spectrometer (ESCALAB 250Xi, Thermo Fisher Scientific Co., Ltd). The Fourier transform infrared spectroscopy (FT-IR) spectrum of hydrogels was recorded by an infrared spectrometer (PerkinElmer Spectrum Two). X-Ray diffraction (XRD) of hydrogels was performed by an X-ray diffractometer (Rigaku Smartlab 9 kW, Nihon Rigaku Co., Ltd).

**3.3.2. Mechanical properties of LM hydrogel.** LM hydrogel-*n* (*n* = 0, 0.6, 0.8, 1.0, and 1.5) was cut into 60 mm × 5 mm × 2 mm (length × width × thickness) strips and then stretched under an electronic universal testing machine (AG-50, Shimadzu Corporation) at a speed of 50 mm min$^{-1}$. And the strain was monitored with a full-field strain measurement system (DIC-12M, LIVOTEK Technology Ltd). LM hydrogel-1.0 strips were stretched at 100%, 200%, 300%, 400%, and 500% and repeated once to create cyclic loading curves. The LM hydrogel-1.0 strip was stretched at 400% and rested for 0, 5, 15, 30, and 60 min to characterize the recovery of LM hydrogel-1.0. The LM hydrogel-1.0 strip was stretched 50 times at 200% strain, and the stress change at 200% strain was observed to characterize the mechanical stability of LM hydrogel-1.0. LM hydrogel-1.0 was made into a cylinder of 20 mm × 20 mm (diameter × height) and compressed under a universal testing machine at a speed of 5 mm min$^{-1}$. LM hydrogel-1.0 was compressed 50 times reciprocally at a speed of 5 mm min$^{-1}$ and a strain of 30%. The LM hydrogel-*n* (*n* = 0 or 1.0) strips were notched by 1/3 width and then stretched to characterize the effect of EGaIn microspheres on the notch sensitivity of the hydrogel. LM hydrogels were made into 10 mm × 5 mm (diameter × height) cylinders and characterized by a dynamic thermomechanical analyzer (Pyris Diamond DMA, PerkinElmer instruments).

**3.3.3. Self-healing properties of LM hydrogel.** The LM hydrogel-1.0 strips were cut diagonally and aligned, self-healed at 25 °C and 98% humidity for 3, 6, 16, and 24 h, and stretched under the electronic universal testing machine at 50 mm min$^{-1}$. In addition, the conductivity of LM hydrogel-1.0 strips was measured before and after cutting and contacting to investigate its conductive self-healing ability.

**3.3.4. Electrical properties of LM hydrogel.** LM hydrogel-*n* (*n* = 0, 0.6, 0.8, 1.0, and 1.5) was cut into 60 mm × 5 mm × 2 mm (length × width × thickness) strips and their conductivity was measured with an electrochemical workstation (Shanghai Chenhua Instrument Co., Ltd). In addition, the resistance of hydrogels was measured during stretching to investigate the gauge factor (GF) of each group of hydrogels. GF is calculated by the following formula:

$$\frac{\Delta R}{R_0} = \frac{R - R_0}{R_0} \times 100\%$$

$$\mathrm{GF} = \left(\frac{\Delta R_2}{R_0} - \frac{\Delta R_1}{R_0}\right) \Big/ (\varepsilon_2 - \varepsilon_1)$$

where $R_0$ is the initial resistance of the LM hydrogel and $R$ is the resistance after stretching. $\varepsilon$ is the stretching strain of the LM hydrogel. The LM hydrogel-1.0 strips were stretched six times at 10%, 20%, 30%, 100%, 200%, and 300%, and the resistance changes were recorded to investigate the potential of LM hydrogel-1.0 as the sensor. The LM hydrogel-1.0 strip was stretched back and forth 200 times with a strain of 200% to investigate the conductivity stability of LM hydrogel-1.0. LM hydrogel-1.0 was made into a cylinder of 20 mm × 20 mm (diameter × height) and compressed by 10%, 20%, 30%, 40%, 50%, and 60% at 5 mm min$^{-1}$ and held for 20 seconds. The currents were measured with an electrochemical workstation.

The LM hydrogel-1.0 strip is connected with wires at both ends and encapsulated with 3 M tape to produce the sensor that can be attached to fingers, arms, knees, foreheads, and faces to detect various movements of the human body. The 40 mm × 40 mm LM hydrogel-1.0 is encapsulated in PDMS and placed under the paper to detect the resistance change caused by the pressure change when writing. The LM hydrogel-1.0 strip is glued to a rubber glove and connected to an LCD, which displays the number represented by the finger to prepare a smart glove for human–computer interaction.

**3.3.5. Infrared camouflage properties.** A 20 mm × 20 mm× 1 mm (length × width × thickness) hydrogel film was prepared, and the dynamic infrared camouflage performance of the LM hydrogel was demonstrated by irradiating it with an 808 nm NIR laser and monitoring the temperature change with infrared thermography. The hydrogel films of 20 mm × 20 mm × 1 mm (length × width × thickness) were prepared and coated with liquid metal on one surface, placed on a thermal bench at 30, 45, and 60 °C, and monitored for temperature changes with infrared thermography to characterize the static infrared camouflage performance of LM hydrogel films with a liquid metal coating.

## 4. Conclusions

In this work, a super-stretchable and self-healing liquid metal/polyvinyl alcohol/P(acrylamide-*co*-octadecyl methacrylate) (liquid metal/PVA/P(AAm-*co*-SMA)) double network hydrogel (LM hydrogel) was successfully fabricated *via* a simple one-pot method for human–computer interaction and infrared camouflage. The gallium-based liquid metal (EGaIn) microspheres not only acted as an initiator to build a ductile P(AAm-*co*-SMA) hydrophobic association network but also yielded coordination interactions with PVA microcrystalline network and hydrogen bonds with P(AAm-*co*-SMA) network, leading to multiple physical cross-links within the LM hydrogel and the resultant excellent mechanical

performance (super-stretchability (2000%), toughness (3.00 MJ $m^{-3}$) and notch resistance). Due to the reversibility and reconstruction of physical cross-links, the LM hydrogel displayed impressive self-healing properties (healing efficiency > 99% after 24 h) and attractive recyclability. The sensitivity of the LM hydrogel on strain detection exceeded that of most reported hydrogels, and the assembled sensor was capable of accurately converting gestures into numbers for human–computer interaction. Additionally, the LM hydrogel can also be utilized in infrared camouflage due to the excellent photothermal effect and low infrared emissivity of the incorporated liquid metal. This work opens up new avenues to prepare super-stretchable, toughness, notch resistance, self-healing, photothermal, and conductive hydrogels for human–computer interaction and infrared camouflage, sketching a promising future for them in intelligent devices and military fields in modern technologies.

## Author contributions

X. L. and Y. Y. conceived the idea. X. L., M. J., Y. D., and X. D. performed the experimental studies. X. L., Y. D., C. X., and Y. W. analyzed the data and drew the scheme diagram. Y. Y., Y. Z., K. Z., X. L., L. C, Y. G., X. T., and X. Z. supervised the work. X. L. wrote the manuscript. X. L., Y. D., Y. Y., Y. Z., and X. Z. revised the manuscript. All authors read the manuscript.

## Conflicts of interest

The authors declare no competing financial interests. All experiments sought the unity of volunteers and did not cause harm to volunteers.

## Acknowledgements

This work was supported by the National Natural Science Foundation of China (No. U21A2094), CASHIPS Director's Fund (YZJJZX202015, YZJJ202304-CX), Natural Science Foundation of China (52173144 and 51803188).

## References

1 O. Erol, A. Pantula, W. Liu and D. H. Gracias, *Adv. Mater. Technol.*, 2019, **4**, 1900043.
2 L. Das, P. Das, A. Bhowal and C. Bhattachariee, *Environ. Technol. Innovation*, 2020, **18**, 100664.
3 S. Farris, K. M. Schaich, L. Liu, L. Piergiovanni and K. L. Yam, *Trends Food Sci. Technol.*, 2009, **20**, 316–332.
4 G. Sharma, B. Thakur, M. Naushad, A. Kumar, F. J. Stadler, S. M. Alfadul and G. T. Mola, *Environ. Chem. Lett.*, 2017, **16**, 113–146.
5 G. Sharifzadeh and H. Hosseinkhani, *Adv. Healthcare Mater.*, 2017, **6**, 1700801.
6 H. Zhao, M. Liu, Y. Zhang, J. Yin and R. Pei, *Nanoscale*, 2020, **12**, 14976–14995.
7 Z. Mohammadi, S. Shangbin, C. Berkland and J. T. Liang, *Chem. Eng. J.*, 2017, **307**, 496–502.
8 B. Liu, W. Huang, G. Yang, Y. An, Y. Yin, N. Wang and B. Jiang, *Mater. Sci. Eng., C*, 2020, **116**, 111259.
9 L. Chen, W. Hu, M. Du, Y. Song, Z. Wu and Q. Zheng, *ACS Appl. Mater. Interfaces*, 2021, **13**, 42240–42249.
10 Y. W. Lee, S. Chun, D. Son, X. Hu, M. Schneider and M. Sitti, *Adv. Mater.*, 2022, **34**, 2109325.
11 D. Mawad, A. Lauto and G. G. Wallace, *Polymeric Hydrogels as Smart Biomaterials*, 2016, ch. 2, pp. 19–44, DOI: **10.1007/978-3-319-25322-0_2**.
12 Z. Wang, Y. Cong and J. Fu, *J. Mater. Chem. B*, 2020, **8**, 3437–3459.
13 Y. Zhou, C. Wan, Y. Yang, H. Yang, S. Wang, Z. Dai, K. Ji, H. Jiang, X. Chen and Y. Long, *Adv. Funct. Mater.*, 2019, **29**, 1806220.
14 H. Liu, X. Wang, Y. Cao, Y. Yang, Y. Yang, Y. Gao, Z. Ma, J. Wang, W. Wang and D. Wu, *ACS Appl. Mater. Interfaces*, 2020, **12**, 25334–25344.
15 F. Fei, P. Kotak, L. He, X. Li, C. Vanderhoef, C. Lamuta and X. Song, *Adv. Funct. Mater.*, 2021, **31**, 2105528.
16 F. Fu, Z. Chen, H. Wang, C. Liu, Y. Liu and Y. Zhao, *Nanoscale*, 2019, **11**, 10846–10851.
17 S. Xia, Q. Zhang, S. Song, L. Duan and G. Gao, *Chem. Mater.*, 2019, **31**, 9522–9531.
18 P. Rahmani and A. Shojaei, *Polymer*, 2022, **254**, 125037.
19 Y. Zhang, M. Song, Y. Diao, B. Li, L. Shi and R. Ran, *RSC Adv.*, 2016, **6**, 112468–112476.
20 B. Yuan, Z. He, W. Fang, X. Bao and J. Liu, *Sci. Bull.*, 2015, **60**, 648–653.
21 T. Daeneke, K. Khoshmanesh, N. Mahmood, I. A. de Castro, D. Esrafilzadeh, S. J. Barrow, M. D. Dickey and K. Kalantar-zadeh, *Chem. Soc. Rev.*, 2018, **47**, 4073–4111.
22 K. Kalantar-Zadeh, J. Tang, T. Daeneke, A. P. O'Mullane, L. A. Stewart, J. Liu, C. Majidi, R. S. Ruoff, P. S. Weiss and M. D. Dickey, *ACS Nano*, 2019, **13**, 7388–7395.
23 N. Ning, W. Huang, S. Liu, Q. Zhao, H. Zou, B. Yu, M. Tian and L. Zhang, *Composites, Part B*, 2019, **179**, 107492.
24 H. Wang, W. Xing, S. Chen, C. Song, M. D. Dickey and T. Deng, *Adv. Mater.*, 2021, **33**, 2103104.
25 H. Ge, H. Li, S. Mei and J. Liu, *Renewable Sustainable Energy Rev.*, 2013, **21**, 331–346.
26 J.-H. Kim, S. Kim, J.-H. So, K. Kim and H.-J. Koo, *ACS Appl. Mater. Interfaces*, 2018, **10**, 17448–17454.
27 Y. Lin, Y. Liu, J. Genzer and M. D. Dickey, *Chem. Sci.*, 2017, **8**, 3832–3837.
28 X. Li, X. Ding, Y. Du, C. Xiao, K. Zheng, X. Liu, X. Tian and X. Zhang, *ACS Omega*, 2022, **7**, 7912–7919.
29 N. Kazem, M. D. Bartlett and C. Majidi, *Adv. Mater.*, 2018, **30**, 1706594.
30 Y. Hu, H. Zhuo, Y. Zhang, H. Lai, J. Yi, Z. Chen, X. Peng, X. Wang, C. Liu, R. Sun and L. Zhong, *Adv. Funct. Mater.*, 2021, **31**, 2106761.
31 Y. Qi, T. Jin, K. Yuan, J. You, C. Shen and K. Xie, *J. Mater. Sci. Technol.*, 2022, **127**, 144–152.
32 J. Yan, X. Zhang, Y. Liu, Y. Ye, J. Yu, Q. Chen, J. Wang, Y. Zhang, Q. Hu, Y. Kang, M. Yang and Z. Gu, *Nano Res.*, 2019, **12**, 1313–1320.

 

33 R. Guo, Y. Zhen, X. Huang and J. Liu, *Appl. Mater. Today*, 2021, **25**, 101236.
34 L. Wang, M. Wang, J. Lu, R. E. A. Ardhi, J. Liu, G. Liu and J. K. Lee, *J. Taiwan Inst. Chem. Eng.*, 2019, **95**, 202–207.
35 I. D. Joshipura, H. R. Ayers, G. A. Castillo, C. Ladd, C. E. Tabor, J. J. Adams and M. D. Dickey, *ACS Appl. Mater. Interfaces*, 2018, **10**, 44686–44695.
36 J. Thelen, M. D. Dickey and T. Ward, *Lab Chip*, 2012, **12**, 3961–3967.
37 M. Liao, H. Liao, J. Ye, P. Wan and L. Zhang, *ACS Appl. Mater. Interfaces*, 2019, **11**, 47358–47364.
38 J. Ma, Y. Lin, Y. W. Kim, Y. Ko, J. Kim, K. H. Oh, J. Y. Sun, C. B. Gorman, M. A. Voinov, A. I. Smirnov, J. Genzer and M. D. Dickey, *ACS Macro Lett.*, 2019, **8**, 1522–1527.
39 X. Li, X. Ding, Y. Du, C. Xiao, Y. Wang, K. Zheng, X. Liu, L. Chen, X. Tian and X. Zhang, *J. Mater. Chem. C*, 2022, **10**, 14255–14264.
40 C. M. Hassan and N. A. Peppas, *Macromolecules*, 2000, **33**, 2472–2479.
41 M. Wang, X. Feng, X. Wang, S. Hu, C. Zhang and H. Qi, *J. Mater. Chem. A*, 2021, **9**, 24539–24547.
42 N. Jonathan, *J. Mol. Spectrosc.*, 1961, **6**, 205–214.
43 Z. Al-Ghaus, A. Akbarinejad, B. Zhu and J. Travas-Sejdic, *J. Mater. Chem. A*, 2021, **9**, 20783–20793.
44 S. Zhang, E. Duque-Redondo, A. Kostiuchenko, J. S. Dolado and G. Ye, *Cem. Concr. Res.*, 2021, **145**, 106452.
45 Z. Li, W. Xu, X. Wang, W. Jiang, X. Ma, F. Wang, C. Zhang and C. Ren, *Eur. Polym. J.*, 2021, **146**, 110253.
46 Z. Li, D. Wang, H. Bai, S. Zhang, P. Ma and W. Dong, *Macromol. Mater. Eng.*, 2019, **305**, 1900623.
47 L.-Y. Zeng, X.-C. Wang, Y. Wen, H.-M. Chen, H.-L. Ni, W.-H. Yu, Y.-F. Bai, K.-Q. Zhao and P. Hu, *Carbohydr. Polym.*, 2023, **300**, 120229.
48 D. Zhang, J. Jian, Y. Xie, S. Gao, Z. Ling, C. Lai, J. Wang, C. Wang, F. Chu and M.-J. Dumont, *Chem. Eng. J.*, 2022, **427**, 130921.
49 Y. Yang, M. Zhou, J. Peng, X. Wang, Y. Liu, W. Wang and D. Wu, *Carbohydr. Polym.*, 2022, **276**, 118753.
50 S. Wang, L. Wang, X. Qu, B. Lei, Y. Zhao, Q. Wang, W. Wang, J. Shao and X. Dong, *ACS Appl. Mater. Interfaces*, 2022, **14**, 50256–50265.
51 M. Wang, H. Chen, X. Li, G. Wang, C. Peng, W. Wang, F. Zhang, J. Wang, H. Liu, G. Yan and H. Qin, *J. Mater. Chem. A*, 2022, **10**, 24096–24105.
52 C. Liu, R. Zhang, P. Li, J. Qu, P. Chao, Z. Mo, T. Yang, N. Qing and L. Tang, *ACS Appl. Mater. Interfaces*, 2022, **14**, 26088–26098.
53 J. Cui, J. Chen, Z. Ni, W. Dong, M. Chen and D. Shi, *ACS Appl. Mater. Interfaces*, 2022, **14**, 47148–47156.
54 Q. Zhang, Q. Wang, G. Wang, Z. Zhang, S. Xia and G. Gao, *ACS Appl. Mater. Interfaces*, 2021, **13**, 50411–50421.
55 Y. Yang, Y. Yang, Y. Cao, X. Wang, Y. Chen, H. Liu, Y. Gao, J. Wang, C. Liu, W. Wang, J.-K. Yu and D. Wu, *Chem. Eng. J.*, 2021, **403**, 126431.
56 T. Wang, X. Ren, Y. Bai, L. Liu and G. Wu, *Carbohydr. Polym.*, 2021, **254**, 117298.
57 Q. Wang, Q. Zhang, G. Wang, Y. Wang, X. Ren and G. Gao, *ACS Appl. Mater. Interfaces*, 2021, **14**, 1921–1928.
58 J. Ren, Y. Liu, Z. Wang, S. Chen, Y. Ma, H. Wei and S. Lü, *Adv. Funct. Mater.*, 2021, **32**, 2107404.
59 F. Mo, Z. Wang, R. Jiang, W. Gai, Q. Li, S. Lv and C. Zhi, *Sci. China Mater.*, 2021, **64**, 2764–2776.
60 W. Ma, W. Cao, T. Lu, Z. Jiang, R. Xiong, S. K. Samal and C. Huang, *ACS Appl. Mater. Interfaces*, 2021, **13**, 58048–58058.
61 C. Liu, X. Wang, H. J. Zhang, X. You and O. Yue, *ACS Appl. Mater. Interfaces*, 2021, **13**, 36240–36252.
62 J. Xu, Z. Wang, J. You, X. Li, M. Li, X. Wu and C. Li, *Chem. Eng. J.*, 2020, **392**, 123788.
63 H. Liu, X. Wang, Y. Cao, Y. Yang, Y. Yang, Y. Gao, Z. Ma, J. Wang, W. Wang and D. Wu, *ACS Appl. Mater. Interfaces*, 2020, **12**, 25334–25344.
64 H. Peng, Y. Xin, J. Xu, H. Liu and J. Zhang, *Mater. Horiz.*, 2019, **6**, 618–625.
65 Y. Gao, J. Peng, M. Zhou, Y. Yang, X. Wang, J. Wang, Y. Cao, W. Wang and D. Wu, *J. Mater. Chem. B*, 2020, **8**, 11010–11020.
66 S. He, B. Guo, X. Sun, M. Shi, H. Zhang, F. Yao, H. Sun and J. Li, *ACS Appl. Mater. Interfaces*, 2022, **14**, 45869–45879.
67 Z. Lei, B. Wu and P. Wu, *Research*, 2021, **2021**, 4515164.